RESEARCH ARTICLE
SOLID EARTH: SEISMOLOGY

Earth and Planetary Physics
3: 510–525, 2019
doi: 10.26464/epp2019052

Possible link between long-term and short-term water injections and earthquakes in salt mine and shale gas site in Changning, south Sichuan Basin, China

XingLin Lei[1*], ZhiWei Wang[1,2], and JinRong Su[3]

[1]Geological Survey of Japan, AIST, Ibaraki 305-8567, Japan;

[2]State Key Laboratory of Earthquake Dynamics, Institute of Geology, China Earthquake Administration, Beijing 100029, China;

[3]Earthquake Monitoring Centre, Sichuan Earthquake Administration, Chengdu 610041, China

Abstract: Late at night on 17 June 2019, a magnitude 6.0 earthquake struck Shuanghe Town and its surrounding area in Changning County, Sichuan, China, becoming the largest earthquake recorded within the southern Sichuan Basin. A series of earthquakes with magnitudes up to 5.6 occurred during a short period after the mainshock, and we thus refer to these earthquakes as the Changning *M*6 earthquake sequence (or swarm). The mainshock was located very close to a salt mine, into which for ~3 decades fresh water had been extensively injected through several wells at a depth of 2.7–3 km. It was also near (within ~15 km) the epicenter of the 18 December 2018 *M*5.7 Xingwen earthquake, which is thought to have been induced by shale gas hydraulic fracturing (HF), prompting questions about the possible involvement of industrial activities in the *M*6 sequence. Following previous studies, this paper focuses on the relationship between injection and seismicity in the Shuanghe salt field and its adjacent Shangluo shale gas block. Except for a period of serious water loss after the start of cross-well injection in 2005–2006, the frequency of earthquakes shows a slightly increasing tendency. Overall, there is a good correlation between the event rate in the Shuanghe area and the loss of injected water. More than 400 $M \geq 3$ earthquakes, including 40 $M \geq 4$ and 5 $M \geq 5$ events, had been observed by the end of August 2019. Meanwhile, in the Shangluo area, seismicity has increased during drilling and HF operations (mostly in vertical wells) since about 2009, and dramatically since the end of 2014, coincident with the start of systematic HF in the area. The event rate shows a progressively increasing background with some fluctuations, paralleling the increase in HF operations. More than 700 $M \geq 3$ earthquakes, including 10 $M \geq 4$ and 3 $M \geq 5$ in spatially and temporally clustered seismic events, are correlated closely with active fracturing platforms. Well-resolved centroid moment tensor results for $M \geq 4$ earthquakes were shown to occur at very shallow depths around shale formations with active HF, in agreement with some of the clusters, which occurred within the coverage area of temporary or new permanent monitoring stations and thus have been precisely located. After the Xingwen *M*5.7 earthquake, seismic activity in the salt well area increased significantly. The Xingwen earthquake may have created a unidirectional rupture to the NNW, with an end point close to the NW-trending fault of the Shuanghe earthquake. Thus, a fault in the Changning anticline might have terminated the fault rupture of the Xingwen earthquake, possibly giving the Xingwen earthquake a role in promoting the Changning *M*6 event.

Keywords: Changning earthquake; injection-induced earthquake; deep well injection; hydraulic fracturing; salt well mine; shale gas

Citation: Lei, X. L., Wang, Z. W., and Su, J. R. (2019). Possible link between long-term and short-term water injections and earthquakes in salt mine and shale gas site in Changning, south Sichuan Basin, China. *Earth Planet. Phys.*, *3*(6), 510–525.
http://doi.org/10.26464/epp2019052

1. Introduction

In the Sichuan Basin of China, both long-term injections (of durations ranging from a few years to several tens of years) for disposal of wastewater (Lei XL et al., 2013, 2008, Zhang ZW et al., 2012) and for deep-well salt mining (Ruan X et al., 2008, Sun XL et al., 2017), and short-term injections (of several months' duration) for shale gas hydraulic fracturing (HF) (Lei XL et al., 2017b, 2019, Meng LY et al., 2019), have caused palpable induced seismicity, resulting in sizable earthquakes up to *M*5.7. Similar to other sites (Atkinson et al., 2016), a high level of HF-induced seismicity and moderate magnitude earthquakes have been limited to some sites in the Sichuan Basin. Among these several injection sites, the long-term injection into a deep well in the Changning Shuanghe salt mine (Ruan X et al., 2008, Sun XL et al., 2017) and HF in the Changning Shangluo shale gas block (Lei XL et al., 2017b, 2019, Meng LX et al., 2019) have demonstrated the highest level of induced seismicity (Figures 1–3). Following the *M*5.7 Xingwen earthquake on 18 Dec. 2018, which appears to have been induced by HF activities, a magnitude 6.0 earthquake struck a wide region centered on Shuanghe Town, Changning County, late at night on 17 June 2019.

Correspondence to: X. L. Lei, xinglin-lei@aist.go.jp
Received 05 OCT 2019; Accepted 01 NOV 2019.
Accepted article online 08 NOV 2019.

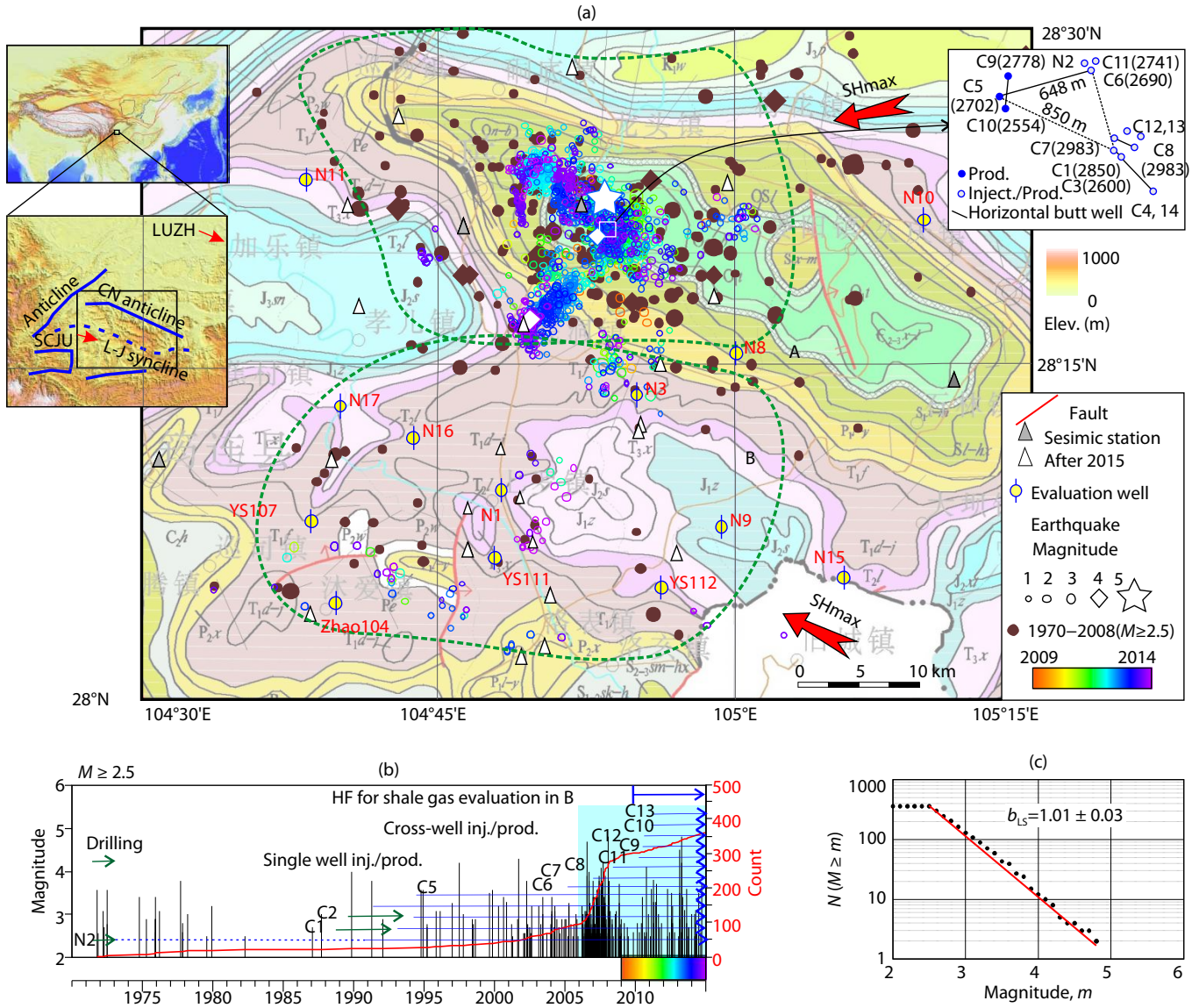

Figure 1. (a) Map of seismic stations, salt mine wells, and earthquakes observed from 1970 through 2014. The large red arrows show the orientations of the maximum horizontal principal stress (SHmax) obtained by this study. In the lower index map, red arrows indicate crust movement at 2 GNSS (Global Navigation Satellite System) stations (LUZH and SCJU) (CENC, 2018) and blue lines indicate axes of major anticlines and a syncline, notably the Changning (CN) anticline and the Luochang–Jianwu (L–J) anticline. A and B indicate the focused areas of this study, Shuanghe and Shangluo, respectively. The background geological map is cut from the 1:500000 digital geologic map (SGS, 2001). Red texts are names of the evolution wells. C# in the zoomed map of the Shuanghe salt mine site represents the name of each production/injection well, and the number in parentheses indicates the depth of the well. (b) Magnitude and accumulated number (red line) of $M \geq 2.5$ earthquakes over time, overlaid on injection periods in the area. (c) Frequency-magnitude distribution (black dots) and seismic b-value (b_{LS}) estimated by the least square method (red lines).

Major tectonic structures in the Shuanghe salt field and its adjacent Changning shale gas block are the Changning anticline ("CN" in Figures 1 and 2) and the Luochang-Jianwu syncline ("L-J" in Figures 1 and 2). The Changning anticline, located in the fold zone of the south boundary of the Sichuan Basin, China, is a SE-extending asymmetric anticline. The NE wing is very steep, with NW-striking faults exhibiting different dip angles. The SW wing is less steep and connected to the Luochang syncline, which is a wide and flat syncline. Superposition of multiple periods of tectonic movements has resulted in complicated structures with several fault systems developed during different geological ages. A NE-extending small anticline, the Shuanghe Town anticline, is overlaid on the Changning anticline. Some NE–NEE-striking faults have also been mapped. At the west end, the Changning anticline bends toward the NW; this bent anticline, where NE-striking faults are dominant, is also known as the Baixiangya anticline. West of the Changning anticline are a number of NE-extending, parallel, and very long fold zones (see the index map in Figure 1). Due to changes in the regional stress field, most faults are unfavorably orientated for rupturing under the present-day regional stress

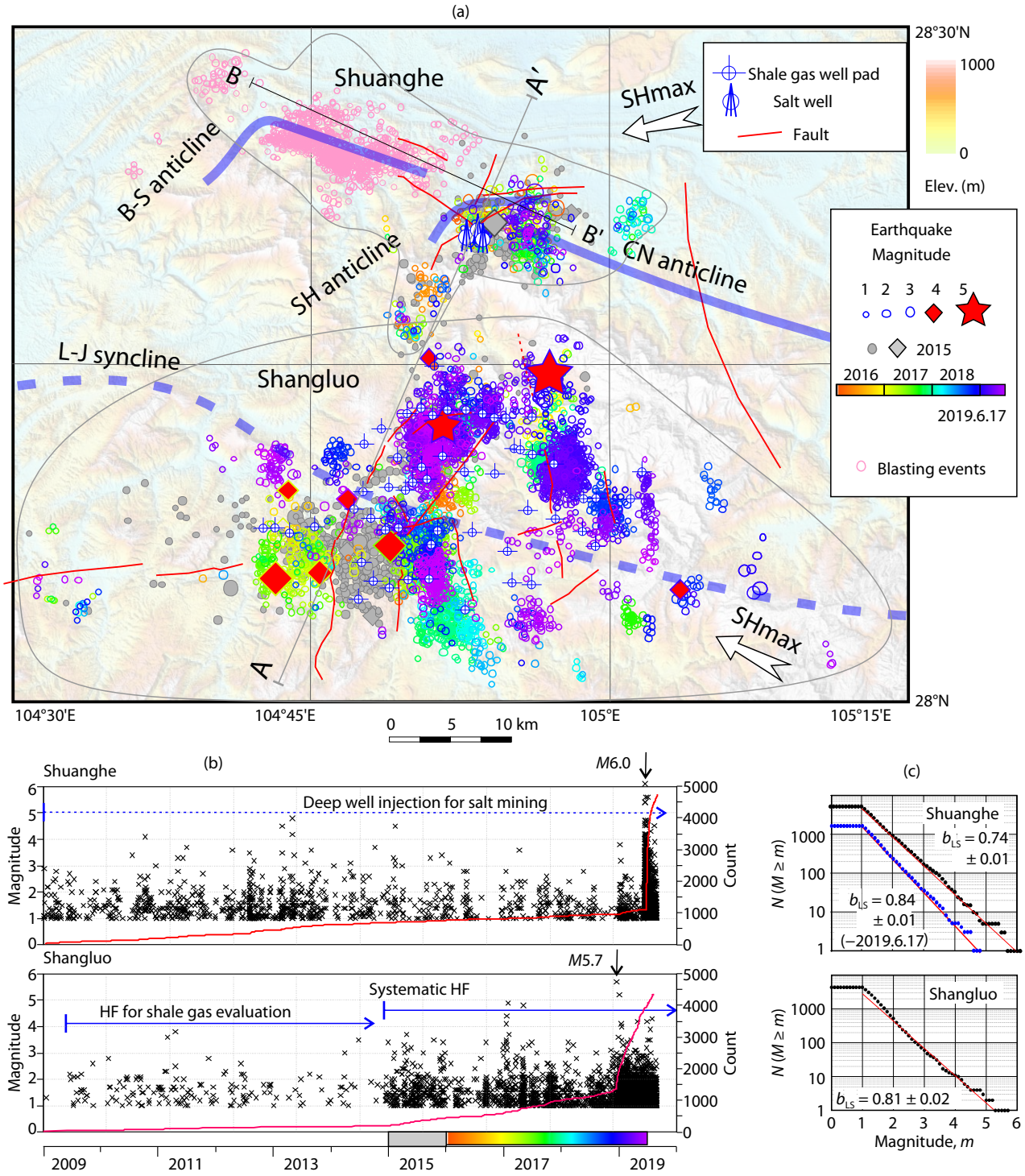

Figure 2. (a) Map of major structures, well pads for shale gas and salt mines, and earthquake hypocenters observed since 2015 in Shuanghe–Shangluo and surrounding areas. "L–J", "B–S", "CN", and "SH" indicate "Luochang–Jianwu", "Baixiangya–Shizitan", "Changning", and "Shuanghe", respectively. (b) Magnitude and accumulated number (red line) of $M \geq 1.0$ earthquakes over time from 2009 to 30 August 2019, overlaid on the injection periods (blue arrows), for the Shuanghe and Shangluo areas. (c) Frequency-magnitude distribution (black dots) and seismic *b*-value (b_{LS}) estimated by the least square method (red lines). For the Shuanghe plot, results for the period from 2000 to the occurrence of the *M*6 Changning earthquake are also shown (blue dots). Note: The original catalog contains many blasting events around a cement plant; they were excluded from this study.

field (Lei XL et al., 2019). As a result, the level of background seismic activity in the area is very low. No earthquakes of magnitude 5 or above appear in the recorded history. The nearest (more than 30 km) earthquakes of *M*5 class are the *M*5.5 Yibin earthquake in 26 BC, the *M*5.5 Gaoxian earthquake in 1610, and the *M*5 Jiang'an earthquake in 1936 (Yi GX et al., 2019). Each of these events oc-

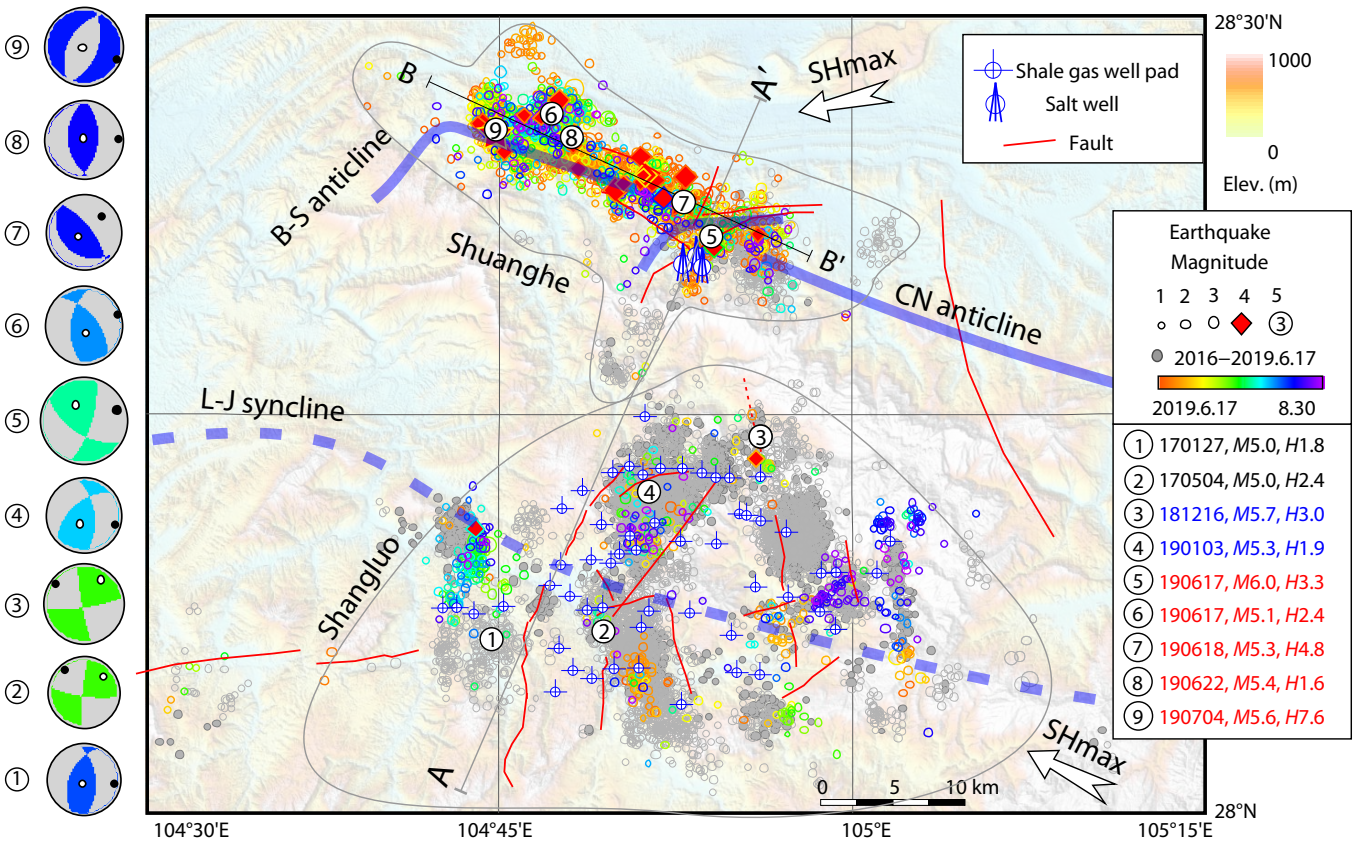

Figure 3. Map of major structures, well pads of shale gas and salt mines, and earthquake hypocenters observed since 2016 in Shuanghe-Shangluo and surrounding areas. Focal mechanisms of $M \geq 5.0$ earthquakes are shown with the lower-hemisphere projection of focal spheres. See caption of Figure 2 for definitions of other texts and symbols.

curred in a different geologic structure. Therefore, the Changning *M*6 and Xingwen *M*5.7 earthquakes set new records for large earthquakes not only within the Changning area but also within the wider region of the entire southern Sichuan Basin. After the mainshock, a series of earthquakes with magnitudes up to 5.6 occurred over a short period, exhibiting typical features of an earthquake swarm. The Changning salt mine is a deep salt well site located in Shuanghe Town, Changning County. The mainshock was located very close to the salt mine, into which fresh water has been extensively injected through several deep wells at a depth of 2.7–3 km for about 30 years. This site is also near (within ~15 km) the epicenter of the *M*5.7 Xingwen earthquake. Questions arose about the possible involvement of industrial activities in these destructive events.

This paper presents some preliminary results of a comparative study examining evidence of a potential link between injections and seismicity in the Shuanghe salt field and its adjacent Changning shale gas block. This is part of an ongoing integrated study on injection-induced seismicity in the southern Sichuan Basin. For convenience, we refer to the Changning *M*6.0 earthquake and its aftershocks as the Changning sequence (swarm). We have divided the study area into two subareas, and refer to them as "Shuanghe" (area A) and "Shangluo" (area B). The Shuanghe area ("A" in Figures 1–3) is in the north and covers the NW portion of the Changning anticline. The Shangluo area ("B" in Figures 1–3) is in the south, and covers the SE portion of the Luochang syncline.

2. Data and Methods

2.1 Data Source

Catalogue data for the period from 1970 through 2008 were downloaded from the China Earthquake Data Center (http://data.earthquake.cn/index.html, in Chinese; login required). Phase and catalogue data (2009–2019.8) used for seismicity analysis and hypocenter relocation were compiled by the Earthquake Monitoring Center, Sichuan Earthquake Administration, China. For the period from January 2016 to Feb. 2017, phase data from Lei XL et al. (2017b), including data from a portable network, were used. Waveform data of $M \geq 4$ earthquakes for moment tensor inversion were provided by Data Management Centre of China National Seismic Network at the Institute of Geophysics, China Earthquake Administration (Zheng XF et al., 2010).

2.2 Hypocenter Relocation

We used catalogue phase data and a hypocenter double-difference (HypoDD) program (Waldhauser and Ellsworth, 2000) to relocate the hypocenters of earthquakes occurring during the period from January 2009 to August 2019. The 1D velocity model was the same as that used in a previous study (Lei XL et al., 2017b). This approach to determine the relative location can improve the relative precision of clustered hypocenters.

2.3 Moment Tensor Inversion

We used the generalized cut and paste (gCAP) method (Zhu LP

and Ben-Zion, 2013), which was advanced in the simultaneous inversion of the full moment tensor and centroid depth using the full waveforms of body and surface waves, to invert the moment tensor of $M_W > 3.5$ earthquakes that occurred in the Shuanghe area. For the Shangluo area, results from a previous study (Lei XL et al., 2019) were used; in this study, we applied the same approach and the same velocity model to the Shuanghe area. The original seismograms were typically filtered with corner frequencies of (0.02, 0.15) or (0.02, 0.1). Full moment tensors were estimated by a grid search with respect to the moment magnitude (steps of 0.01) and the strike, dip, and rake angles (steps of 5 deg) of the faults and slip orientations. The obtained full-moment tensor was decomposed into double-couple (DC), isotropic, and compensated linear vector dipole components (Zhu LP and Ben-Zion, 2013). Because the amplitude spectra of surface waves are very sensitive to source depth, they can be reliably determined by the gCAP method. As presented in Lei XL et al. (2019), uncertainty of the centroid moment tensor (CMT) depth due to velocity error is less than 200–400 m for most events. Indeed, the centroid depth represents the mean depth of major rupture areas during the associated earthquake rather than the faulting nucleation depth.

2.4 Stress Inversion and Estimation of Fluid Overpressure

By assuming that seismic slip occurs in the direction of the resolved shear traction acting on preexisting faults, the crustal stress states can be partly estimated from a variety of focal mechanisms (e.g., Gephart and Forsyth, 1984, Hardebeck and Michael, 2006, Michael, 1987). This standard method can be expanded to an inversion for a regional, possibly varying, stress field. Mean stress in spatial and/or temporal boxes is solved by the damped inversion method, which minimizes the weighted sum of the data misfit and the model length (Hardebeck and Michael, 2006). In this study, we used the least squares method to estimate separately the mean stress patterns for the Shuanghe and Shangluo areas. The uncertainty of the inversion results was estimated through 5,000 Monte Carlo runs by randomly choosing one of the nodal planes to be considered as the source fault.

By further assuming that 1) the occurrence of seismic slip follows the Coulomb failure criterion with a given frictional coefficient, 2) the vertical stress is the weight of the overburden, and 3) optimally oriented faults are critically stressed and aligned to the prevailing regional stress pattern with hydrostatic fluid pressure, it is possible to estimate the Coulomb failure stress (CFS) and the pore overpressure at the source area of earthquakes with well-determined mechanism solutions (Terakawa et al., 2012).

2.5 Fluid Pressure Diffusion Along Two-Dimensional Fracture Surface

Precise estimation of fluid pressure diffusion along complex fracture networks relies on fully coupled simulation, which requires a full set of rock properties, detailed three-dimensional (3D) geological structure (especially the distribution of pre-existing faults), and detailed injection history. As a preliminary analysis, this study makes a rough estimation of pore pressure diffusion along a fault plane based on theoretical solution of a two-dimensional radial flow model of an infinite and isotropic layer. Under the assumption that Darcy's law holds, the pore pressure change from a point source is given (Barker, 1988) as

$$\Delta P(t,r) = Q\frac{\eta}{4\pi kH}\Gamma\left(0,\frac{r^2}{4Dt}\right), \tag{1}$$

$$D = \frac{k}{\eta S_a},\quad S_a = \phi\left(\beta_{fl}+\beta_{pv}\right). \tag{2}$$

In Equations (1) and (2), t is time in seconds since the start of pumping, r is the distance in meters from pumping well, Q is the injection rate (or rate of water loss) in cubic meters per second, H is the layer thickness in meters, K is the layer permeability in square meters, D is hydraulic diffusivity in square meters per second, η is the dynamic viscosity of water in pascal-seconds, S_a is the unconstrained specific storage coefficient (per pascal), β_{fl} is compressibility of the fluid per pascal, and β_{pv} is compressibility of the pores per pascal. The properties of water are $\beta_{fl} = 4\times10^{-10}$ Pa^{-1} and $\eta = 0.001$ Pa·s.

2.6 Coulomb Failure Stress

The CFS transferred from nearby fault slips was calculated based on the Okada dislocation model (Okada, 1992). The elastic medium was assumed to be homogeneous and isotropic with a shear modulus of 32 GPa and Poisson's ratio of 0.25. The Coulomb stress is calculated according to the following equation:

$$\Delta\mathrm{CFS} = \Delta\tau - \mu\left(\Delta\sigma - \Delta P\right), \tag{3}$$

where μ is the frictional coefficient (= 0.6 from experimental results using typical rocks from the Sichuan Basin (Lei XL et al., 2014)); $\Delta\tau$ and $\Delta\sigma$ are changes in the shear and normal stresses, respectively, on given receiver faults for the given strike, dip, and rake; and ΔP is the unrelaxed pore pressure change, which is defined as $\Delta P = B\Delta\sigma_m$, where σ_m is the mean stress and B is Boit's coefficient. In this paper, compressional stress is positive.

3. Results

3.1 Results of Moment Tensor Inversion and Hypocenter Relocation

By the end of August 2019, 11 $M_W > 4$ earthquakes occurred within the Shuanghe area and were recorded by many broadband seismic stations from the regional seismic networks. At first, we inverted the full centroid moment tensor (CMT) using the gCAP method and velocity model as mentioned in Section 2. Table 1 gives a summary of the results. Except for the *M*4.1 event on 12 August 2019, all events revealed almost pure DC mechanisms, showing that the squared ratios of the scalar potency of the non-DC components to the total scalar potency are less than a few percent. The *M*4.1 event is likely to have been a special event with complex sources and processes (the fitting is very poor), and was thus excluded from this study. The centroid focal depths, corresponding to the minimum misfit error, fall in the range from 1.3 to 7.6 km (Table 1).

For the Shangluo shale gas block, results of previous studies were referenced (Lei XL et al., 2017b, 2019). In total, moment tensors of all 18 earthquakes ($M_W > 3.5$) were well determined with a focal

Table 1. Results of focal mechanism solutions of $M_W > 4$ earthquakes during the Changning Shuanghe earthquake swarm obtained using the gCAP method. P_f is fluid overpressure estimated by assuming the specified frictional coefficient

#	Date	M	M_W	H	Fault-1			Fault-2			P_f (μ=0.6)	P_f (μ=0.4)
				(km)	(S, D, R) (deg)			(S, D, R) (deg)			(MPa)	(MPa)
1	06-17 22:55	6.1	5.69	3.3	122	53	28	15	68	140	25.8	15.3
2	06-17 23:36	5.4	5.01	2.0	320	51	59	184	48	122	11.0	5.7
3	06-18 00:29	4.5	4.25	2.0	0	59	155	104	69	34	20.1	10.6
4	06-18 00:37	4.6	4.18	1.3	150	50	79	–13	41	103	1.2	0.1
5	06-18 05:03	4.6	4.42	3.0	130	35	94	–55	55	87	4.5	2.9
6	06-18 07:34	5.4	4.82	4.8	130	23	82	–41	67	93	5.4	9.4
7	06-22 22:29	5.6	5.08	1.6	175	41	85	2	49	94	5.9	2.3
8	06-23 08:28	4.7	4.39	6.5	150	59	26	46	68	146	76.4	66.8
9	07-04 10:17	5.6	5.05	7.6	16	48	81	209	43	100	23.1	12.0
10	07-22 16:26	4.3	4.16	1.4	164	56	81	0	35	103	0.2	0.6

depth in the range from 0.9 to 4 km (Lei XL et al., 2019). All events showed nearly pure DC mechanisms with very limited non-DC components, probably due to uncertainty.

Hypocenter depth is a key issue in the debate over whether an earthquake was induced or not. However, the depth is often the least accurate parameter determined by routine analysis, especially when there are no nearby stations. Approaches to determining relative location, such as the HypoDD method used in this study, can improve the relative precision of the hypocenter depth of clustered earthquakes. In this study, we relocated all M1.0 earthquakes occurring in 2009 and later. For earthquakes before 2009, the original catalog was used. Due to the inhomogeneous distribution of seismic stations, in addition to the fact that some stations were installed after major earthquakes, the final location error depends on time and geographical location. Some large events and all spatially isolated events were excluded from the relocation process. Thus, we used the relocated catalogue only for mapping and the original phase catalogue for statistical analysis. The best relocation precision for earthquakes occurring during the period from 2016 to Feb. 2017 was possible in the center part of the Shangluo area, because of data from a portable seismic network. After the Xingwen M5.7 earthquake, several additional stations were installed in the Shangluo area, and hypocenters of events from February 2019 were determined with even greater precision. Unfortunately, a key station (CNI) closest to the salt mine failed 10 hours before the M6 earthquake; the main event was thus not recorded by this station. However, since the station was repaired 10 minutes after the mainshock, the aftershocks were recorded.

As aforementioned, the travel times of both P and S wave are insensitive to focal depth at distant stations. In contrast, surface waves impose a robust constraint on focal depth estimations, especially for shallow earthquakes. In this study, we preferred to use the CMT depth for large events, as obtained from the gCAP method described in Section 2.3. What needs attention is that the centroid depth is usually different from that when earthquake rupturing started. The difference could reach several kilometers for M5–6 earthquakes, because the rupturing dimension of the source fault ranges from a few kilometers for M5 to ~10 km for M6. Taking the Changning M6.0 earthquake as an example, the CMT depth was 3.3 km, and the relocated focal depth was 5 km (Yi GX et al., 2019) and 9.6 km (this study), suggesting that although this earthquake rupturing shows a weighted mean depth of 3.3 km, it may have been initiated a few kilometers deeper.

Giving the general results, the following subsections present detailed seismic activities and their possible link to injections in the Shuanghe salt mine area and the Shangluo shale gas area for typical time periods.

3.2 Seismicity Between 1970 and 2014

In the Shuanghe salt mine, 14 deep wells were drilled into the rock salt formation at depths ranging from 2,500 to 2,800 m (Figures 1 and 4). The salt mine is developed in the Sinian dolomite formation. Fresh water has been extensively injected into several wells for the purpose of dissolving and producing salt. The mean injection rate was ~50,000 m^3/month in 2001; it increased to ~130,000 m^3/month in 2010, and then it rapidly increased to 200,000 m^3/month because additional wells were used. In 2013, the injection rate reached ~240,000 m^3/month. Data are not available after 2013, but the injection rate must have remained at a similar level because salt production at the mine did not decrease. In August 2019, the pumping station worked at least 10 hours per day with an injection rate of 500–600 m^3/hour (personal communication with local people), resulting in a rough estimation of a rate of ~150,000 m^3/month.

As seen in Figure 1, in the study area, earthquakes occurring in the period from 1970 through 2014 were scattered throughout the Shuanghe area but were concentrated near the salt mine. From the 1970s to the middle 1980s, no earthquakes of magnitude 4 or higher were observed in the area. The few earthquakes were probably related to the installation of the N2 well, which was drilled in 1970–1971 for oil/gas prospecting. Since the end of the 1980s, increasing seismicity has been observed coincident with salt mining by injection and production through individual vertical wells. Several wells were horizontally docked in 2004–2006. Then there was a period with a significantly higher event rate

from April 2006 to the end of 2017 (Figure 1b), closely corresponding to a period of significant injection water loss (as determined by subtracting the production volume from the injected water volume) (Ruan X et al., 2008). In fact, the total water loss for the period from 2000 through 2013 reached 850,000 m^3 (Sun XL et al., 2017), resulting in a mean rate of 0.135 m^3/min. In an overview report, the cumulative earthquake moment was found to be linearly proportional to the cumulative water loss, and it could be modeled by the empirical formula proposed by McGarr (McGarr, 2014) (Sun et al., 2017). This model is expected to work statistically for the mean behavior of many injection wells, but it may fail for individual injection wells (Ellsworth et al., 2019, Lei XL et al., 2019).

Relocated earthquakes for the period from Feb. 2000 to 20 Nov. 2007 show that a focal depth of $h \leq 3$ km accounts for 74.5% of the total. When viewed on a map, earthquake hypocenters are clustered in a northwest-extended zone and more events were located to the southeast of the mining area (Ruan X et al., 2008).

Our relocated earthquake hypocenters for events occurring in 2009 and later demonstrate a "square ruler" shape (Figure 1a). The NW leg extends for ~15 km along the axis of the Changning anticline. The other leg extends for ~15 km along the SW direction. The corner of the "ruler" corresponds to the salt mine location. This pattern of hypocenter distribution indicates that the NW-striking faults along the Changning anticline and the NE-striking faults along the Shuanghe Town anticline were activated.

The Shangluo area, corresponding to the Changning shale gas demonstration block, in which the target Silurian mudstone/shale formation is in the Luochang syncline, has a burial depth from <2 to >3 km. Vertical wells have been drilled for shale gas prospecting since 2008. Horizontal drilling began in 2011, and systematic HF in horizontal wells began in Dec. 2014 (Lei XL et al., 2017b). As seen from Figure 1, in the period from 1970 to Oct. 2008, only a small number of earthquakes with a magnitude less than 4 were observed within the shale gas block, indicating that the area had a low (but non-zero) level of background seismicity. However, after the start of shale gas prospecting in 2008, an increasing event rate appears to have been induced mainly by HF conducted for evaluation purposes (Lei XL et al., 2017b).

In a summary, until 2014, major seismicity was limited in the Shuanghe area. The event rate is clearly correlated with the injection history and water loss in the salt mine. As seen in Figure 1c, the frequency-magnitude relation shows a seismic *b*-value of 1.01, very close to the global mean value. The "expected" maximum magnitude is 5.0, and the observed maximum magnitude is 4.8 during the period.

3.3 Seismicity Since the End of 2014

HF-induced seismicity in the Shangluo area between the end of 2014 and February 2019 has been documented in previous studies (Lei XL et al., 2017b, 2019). Here, we present a brief summary with updated data. In the Changning block, a typical well pad generally has four to eight wellbores with horizontal lengths of 1,000–2,500 m and intervals of 300–400 m between the lateral portions of neighboring wells. A multistage zipper-fracturing technique has normally been applied for treatment. On average, more than 1,800 m^3 of water is required for a single stage. The average wellhead pressure is ~60–70 MPa (Ren R et al., 2015). In the Shangluo area, systematic HF in horizontal wells for shale gas production began at the end of 2014. Since Dec. 2014, the earthquake rate has dramatically increased and a number of event clusters surrounding the hydraulic fracturing well pads have been observed (Figure 2b). A converging chain of evidence, including spatiotemporal correlation between earthquakes and HF zones, statistic parameters of seismicity, and estimated overpressure required to activate the unfavorably oriented source faults of the largest events, suggests that the progressively increasing seismicity has been induced by HF at a depth of approximately 2.5–3 km. Thus far, 11 $M \geq 4.0$ events (including 3 $M \geq 5.0$ events) have been observed since the systematic HF operation began in 2014. From the Gutenberg–Richter frequency-magnitude relation in Figure 2c, the estimated seismic *b*-value is 0.81, significantly lower than that of microseismicity directly caused by hydraulic fracturing. It is not surprising to have some $M \geq 5$ earthquakes, because the expected maximum magnitude is ~5.2. Indeed, the largest event, the *M*5.7 Xingwen earthquake on 16 Dec. 2018, is an outlier or extreme event in that context. The best-fit central moment depth was 3.09 km and the hypocenter was very close to the front of the north-ward horizontal wells of the N201-H24 well pad (Lei XL et al., 2019). HF in N201-H24 began in October 2018 and was completed on 13 January 2019. The faulting rupture of the *M*5.7 earthquake was thus probably initiated within the zone of overpressure and ruptured beyond it.

Between the end of 2014 and the occurrence of the Changning *M*6 earthquakes, many more earthquakes occurred in the east side of the salt field, clustered along the NNW direction (Figure 2). Just before the occurrence of the *M*6 sequence, the estimated seismic *b*-value was ~0.84, and the expected maximum magnitude was ~5.2. Therefore, the *M*6 earthquake is also an extreme event. Moreover, if we add aftershocks, the estimated seismic *b*-value becomes ~0.74, and the expected maximum magnitude is indeed ~6.0. In addition, the maximum aftershock, showing a magnitude of 5.6, is also too large to obey Båth's law (Båth, 1965), which states that the difference in magnitude between a main shock and its largest aftershock, typically 1.1–1.2, is approximately constant, regardless of the mainshock magnitude. The *M*6 event thus triggered many more large aftershocks than expected from a typical main-aftershock sequence.

The distribution of relocated hypocenters shows that earthquakes in Shuanghe and Shangluo remained spatially separated (Figures 2a and 3). However, the SW-extending cluster from the salt mine is a possible bridge connecting the Shangluo and Shuanghe areas. Before the Xingwen *M*5.7 earthquake on 18 Dec. 2018, there was no clear interaction between the seismic activities of Shuanghe and Shangluo. The event rate in Shuanghe was basically stable with a slightly increasing tendency. However, coincident with the Xingwen *M*5.7 event, the event rate in Shuanghe increased by ~3 times until the occurrence of the *M*6 earthquake. It is interesting that the Xingwen *M*5.7 earthquake did not produce as many aftershocks as would be expected based on the modified Omori law (Utsu, 1961) for aftershock decay rates, or af-

tershocks as large as would be expected based on Båth's law for the largest aftershock (Båth, 1965) in the shale gas area. The increasing event rate in the shale gas area since the end of 2018 reflects increasing HF activities (Lei XL et al., 2019).

As aforementioned, except for some clusters and some time periods, the routinely determined hypocenter depth has errors, although relocation has improved location precision but retains error on the order a few kilometers. However, some clusters were relocated more precisely, with error in the order of 100 m. Figure 4 shows simplified geological sections (defined in Figures 2–3) overlaid onto the relocated hypocenters for earthquakes observed for two selected periods, one from 2016 to 2018 (Lei XL et al., 2017b) and another from 1 January 2019 to 16 June 2019. Locations labeled Z1 (in the Shangluo shale gas area) and Z2 (close to the salt mine) in Figure 4 indicate two regions with relatively good seismic station coverage, and thus the hypocenters within these regions are regarded as accurate. In the Z1 region, the hypocenters are distributed within a narrow depth range from 1 to 4 km. Note that the target shale formation here is ~2.5 km deep. In Z2, in which the salt mine has a depth range from 2.7 to 3 km, the relocated hypocenters fall within a depth range from 1 to 6 km. It is impossible to draw the conclusion that other poorly located hypocenters must fall within the same depth ranges. Nevertheless, the accurately determined locations provide good samples for positing the seismic relationship between these regions. It is important to note that the centroid depths of the CMTs accurately resolved by the gCAP method completely fall within the depth ranges of the accurately located clusters.

In summary, between the end of 2014 to the time of the occurrence of the *M*6 earthquake, major seismicity in the Shuanghe area had a slightly increasing event rate until the *M*5.7 Xingwen earthquake occurred in the north part of the Shangluo shale gas area. The *M*5.7 event increased the event rate in the Shuanghe area by several times. Many more earthquakes occurred in the

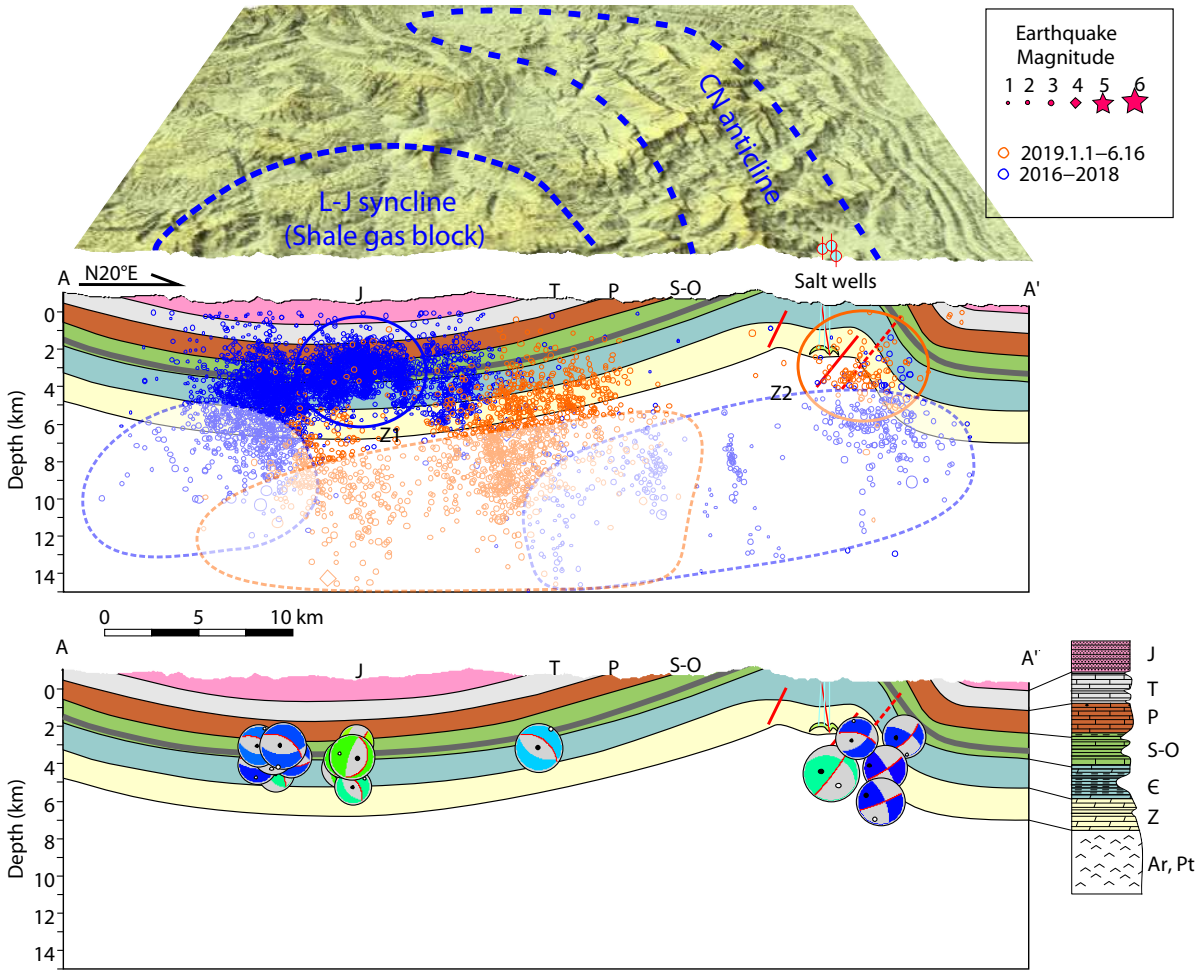

Figure 4. Simplified geological sections (defined in Figures 2–3) overlaid on relocated hypocenters for earthquakes observed from 2015 through 2018 (Lei XL et al., 2017b) and from 1 January 2019 to 31 June 2019. Regions Z1 (Shangluo shale gas area) and Z2 (salt well area) indicate zones in which hypocenter depths were determined precisely because they were centered in either portable or newly added stations. Regions marked by dashed lines indicate zones in which hypocenter depths were poorly determined. Focal mechanisms of M_W > 3.5 earthquakes are shown with the lower-hemisphere projection of focal spheres viewed from the vertical profile. The top 3D shaded image shows the landscape and the syncline and anticline structures. The geological sections were drawn based on the 1:500000 digital geologic map (http://219.142.81.86/igserver/ogc/kvp/TAS10B520000SC/WMTSServer, last accessed Nov. 2019) and sections in Zou CN et al. (2015).

eastern neighboring area of the salt field, extending along the NNW direction, which is also the direction of major clusters in the shale gas area.

3.4 Changning *M*6 Sequence

The Changning *M*6 earthquake occurred at 22:18 local time on 17 June 2019, when people were enjoying the full moon. This event is remarkable in that it is the largest earthquake not only within the Changning district but also in the entire region of the southern Sichuan Basin edge.

Figure 5c presents the hypocenter distribution along a line parallel to the Changning anticline axis. With the assistance of stations installed after the *M*5.7 Xingwen earthquake, the relocated hypocenters are fairly well known. Focal mechanisms of M_W > 3.5 earthquakes are shown with the lower-hemisphere projection of focal spheres viewed from the vertical profile. Both relocated hypocenters and CMT solutions demonstrated a tendency of increasing maximum depth from east to west. On the east side — in other words, the epicentral area of the mainshock — the focal depth is less than 6 km. The maximum hypocenter depth reaches about 12 km in the NW corner of the Changning anticline.

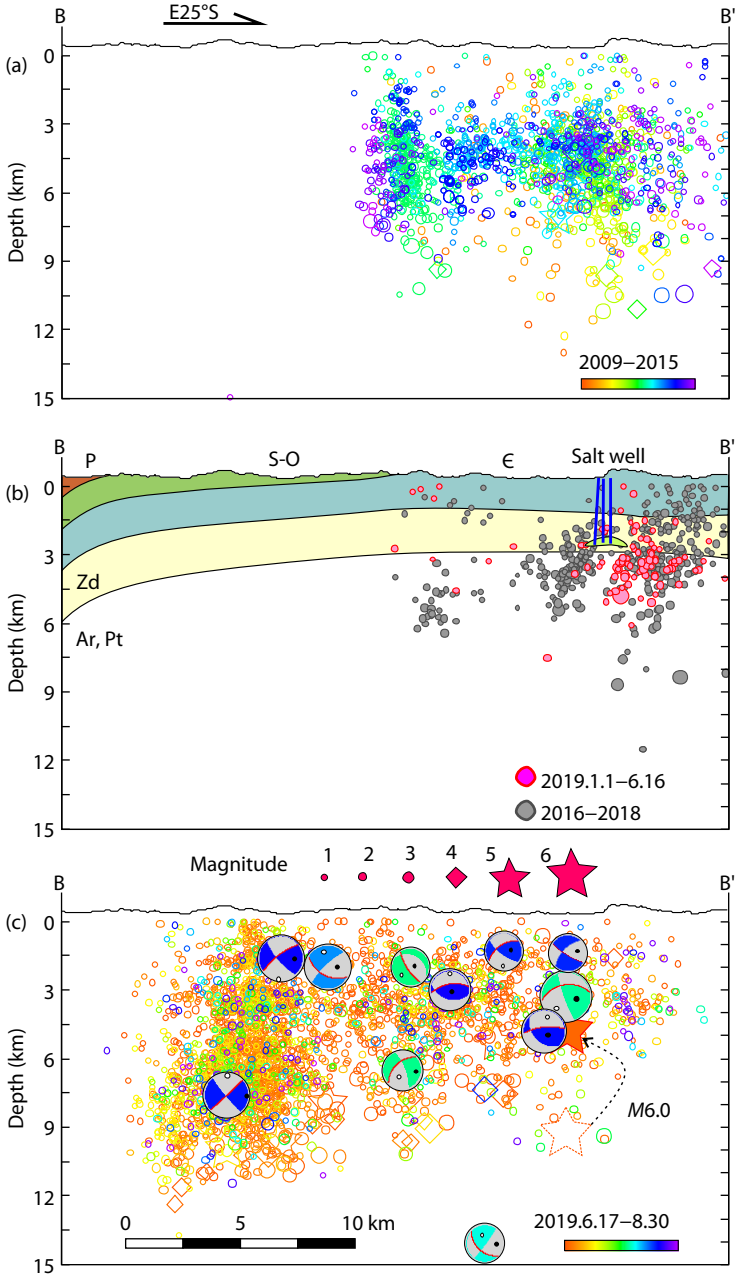

Figure 5. Simplified geological sections (defined in Figure 3) overlaid on relocated hypocenters observed in different periods: (a) 2009–2015, (b) 2016–2018 and 1 January 2019–16 June 2019, and (c) 17 June 2019–30 August 2019. Note that the hypocenters in the left side were more accurately determined than those in the right side. Focal mechanisms of M_W > 4 earthquakes are shown with the lower-hemisphere projection of focal spheres viewed from the vertical profile.

3.5 Stress Transformation

Fault rupturing changes stress in neighboring areas and can trigger earthquakes. It is valuable to examine stress transferred from the *M*5.7 Xingwen earthquake to the source fault of the *M*6 Changning earthquake. Based on the mechanism solution and surface damage, the nodal plane of (strike, dip, rake) = (170°, 83°, 12°) was assumed to be the source fault. The fault area was estimated according to the empirical relationship between the moment magnitude and the rupture dimension: $M_W = \log_{10}A - 2.0$ (where A is the rupture area in square meters) (Leonard, 2010). The slip was calculated from $Mo = GuA$, where Mo is the moment, G is the shear modulus of the elastic medium, and u is the displacement. Figure 6a shows the distribution of ΔCFS, which was calculated for two different receiver faults at a depth of 6 km, overlaid on earthquake hypocenters since January 2019. In the northwest region, the receiver faults are coincident with the source fault of the Changning earthquake. In other regions, the re-

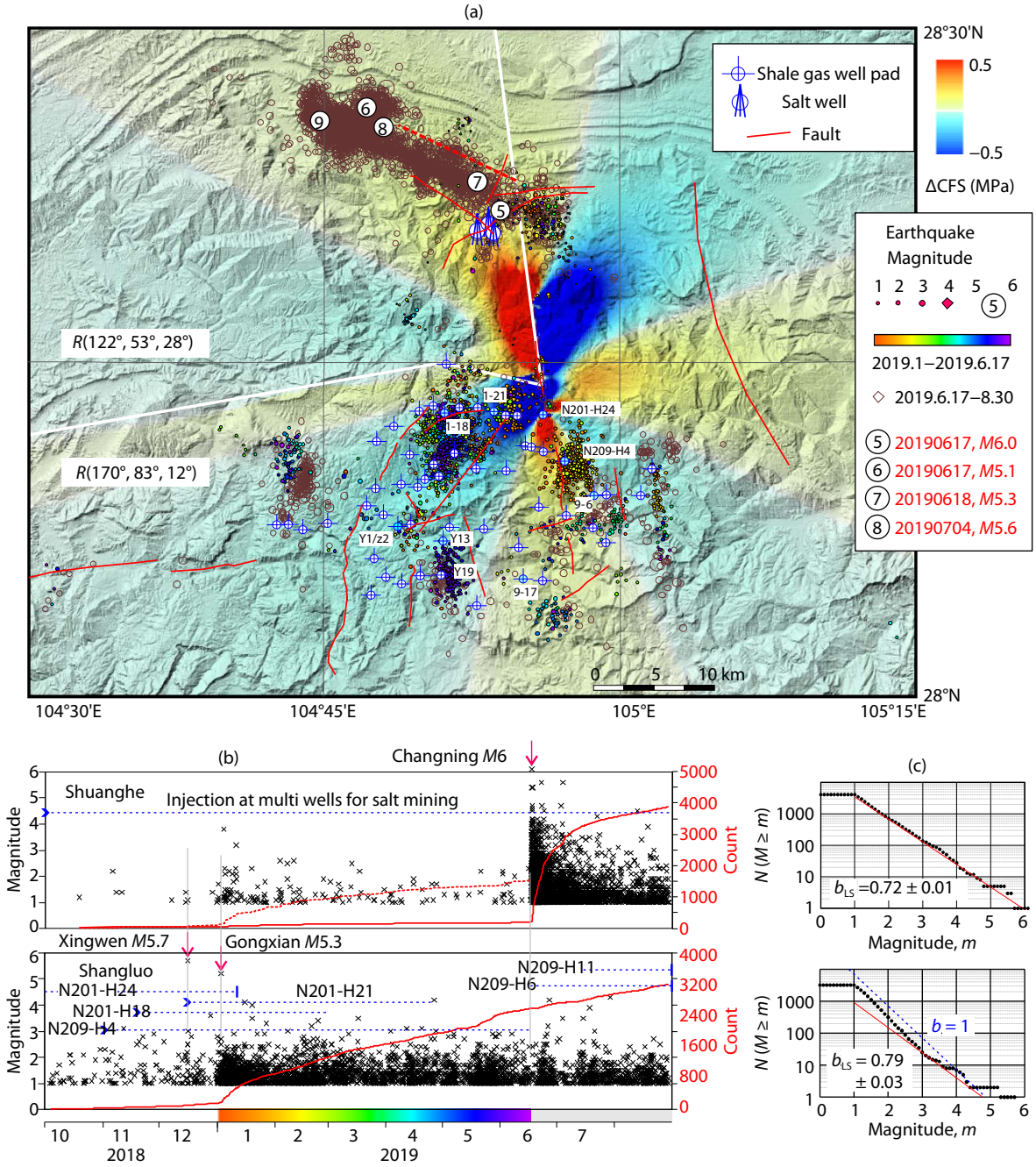

Figure 6. (a) Map showing active faults, active well pads, and earthquake hypocenter distribution from 1 January 2019 to 30 August 2019, overlaid on a background image of Coulomb failure stress (ΔCFS) from the Xingwen *M*5.7 earthquake to receiver faults of *R* (strike, dip, rake) given in the map. (b) Magnitude and accumulated number (red line) of $M \geq 1.0$ earthquakes over time, overlaid on injection periods for the Shuanghe and Shangluo areas. (c) Frequency-magnitude distribution (black dots) and seismic *b*-value (b_{LS}) estimated by the least square method (red lines). For the Shangluo plot, line of $b = 1$ (blue) is plotted for reference.

ceiver faults have the same strike, dip, and rake as the source fault of the Xingwen earthquake because earthquakes are clustered along a direction similar to the strike of the Xingwen earthquake. In the Shangluo shale gas area, more earthquakes were located in regions of negative ΔCFS (Figure 6a). Although the seismic rate increased in February 2019 in the Shangluo area, in agreement with a previous study, seismicity in Shangluo linked to active HF and impaction from the *M*5.7 Xingwen earthquake is less important. The *M*6.0 main earthquake and most "foreshocks" in the Shuanghe area fall into regions of positive ΔCFS. In addition, as aforementioned, a clear increase in seismicity in the Shuanghe area was observed (Figure 6b). Thus, increasing seismicity in the Shuanghe area most probably indicated that the Xingwen *M*5.7 earthquake played a role in promoting the Changning *M*6 earthquake.

Through the end of August 2019, four earthquakes of $M \geq 5$ have been observed. We thus calculated ΔCFS at each hypocenter of the Changning sequence from all $M \geq 5$ earthquakes occurring before the specific event. For each hypocenter, one of the nodal planes of the nearest earthquake having a CMT result was used as the receiver fault. Figure 7 shows the results for CFS, which show that 78% of these earthquakes fall within the area of positive ΔCFS, indicating that these largest events played an important role in triggering the Changning aftershocks.

3.6 Stress Pattern Inversion and Fault Reactivation Analysis

To evaluate the fluid pressure required for fault activation associated with the major earthquakes in the Shuanghe area, we used the stress field inversion approach of Lei XL et al. (2019) to estim-

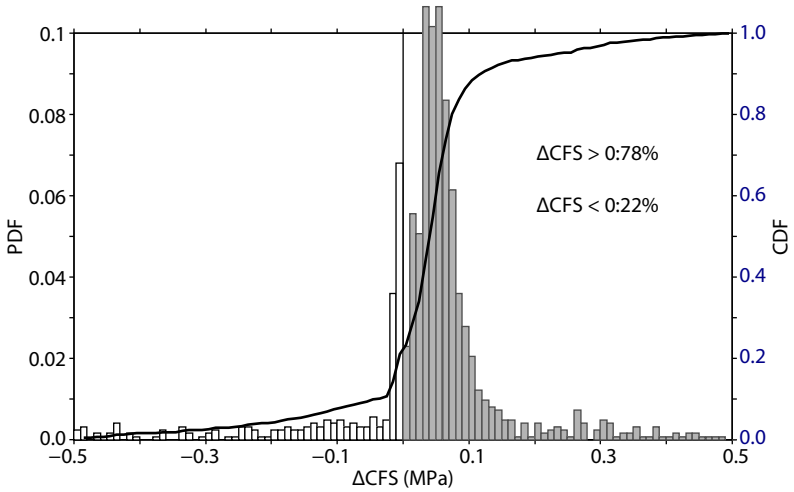

Figure 7. Probability density function (PDF) and cumulative distribution function (CDF) for CFS transferred from the $M \geq 5$ earthquakes and calculated at each hypocenter of the aftershocks of the Changning sequence until 30 August 2019. Stress from the nodal plane giving the greatest ΔCFS for the nearest earthquake having a CMT solution was used as the receiver fault for a given hypocenter. The result is that 78% of earthquakes fall within the area of positive ΔCFS.

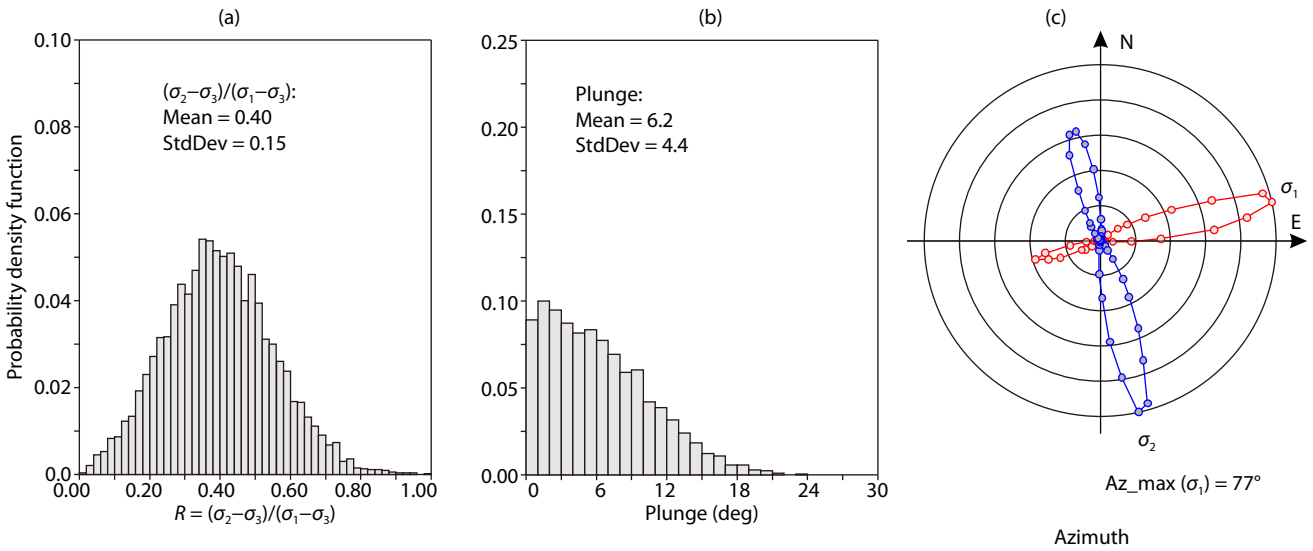

Figure 8. (a) Estimated stress ratio of the principal stresses (σ_1, σ_2, and σ_3) and estimated maximum principal stress axis in terms of (b) plunge angle and (c) azimuth.

ate the CFS and fluid pressure required to cause $M > 4$ earthquakes under a uniform regional stress. In total, 10 CMTs (Table 1) were used. Results of 5,000 Monte Carlo simulations are shown in Figure 8. The obtained orientation (azimuth = 77 deg) of the maximum principal stress axis is consistent with the results obtained by Sun XL et al. (2017) from the focal mechanism of small and medium earthquakes. The mean stress ratio of the maximum principal stresses is $R = 0.4$. As compared with the results for the Shangluo area, both areas show almost horizontal maximum principal stress; however, the stress patterns vary significantly. At first, the direction of the maximum anticlockwise rotated about 40 deg from the syncline to the anticline. Then, the stress ratio increased from 0.15 to 0.4. Under such a stress pattern and assuming critical stress on the favorably oriented faults, the estimated pore pressure (ignoring the poroelastic effect) ranged from 0.1 to 67 MPa. Five of the 10 events show an overpressure less than 10 MPa. Most of the faults in the Shuanghe area are not favorably oriented under the resolved mean stress field and require large fluid pressure or some kind of local load to initiate unstable sliding (Figure 9).

We applied the theoretical solution introduced in Section 2.5 to roughly estimate pure pore diffusion along connected fault networks. The connected faults were simply represented by an infinite fracture plane with a given equivalent thickness of 2 m. The porosity, hydraulic diffusion coefficient, and permeability of the fracture zone were $\phi = 0.15$, $D = 0.1$ m^2/s, and $K = 10^{-14}$ m^2 (corresponding to $\beta_{pv} = 10^{-10}$ Pa^{-1}), respectively. A constant injection rate of 0.135 m^3/min, estimated from water loss over more than 10 years, was used. Because the well head pressure was maintained between 8 and 10 MPa, we assumed a constant injection pressure of 8 MPa. To force both injection rate and pressure to be constant, the source area must grow over time. Under these assumed parameters, the 1-MPa and 8-MPa fronts reached 15 km and 8 km, respectively, after 10 years of injection (Figure 10).

3.7 Results for Other Statistics

In the shale gas area, the stacked hourly distributions show that more events occurred during the daytime than nighttime. Especially during the period from 2009 to 2015, the event rate increased from 8 a.m. and reached the maximum level at ~10 a.m. The level remained at its maximum until 7 p.m., and then gradually decreased to its minimum at 6 a.m. the following day (Figure 11). Such a pattern closely reflects the timing of HF operations at the shale field. This pattern has been observed since 2016; however, the difference between day and night has decreased over time, in agreement with the fact that HF operations have extended into nighttime. But on average, the number of HF operations during daytime remains greater than at nighttime. At the Shuanghe salt mine, the hourly rates were rather irregular, reflecting the fact that the bottom pressure in the wells is controlled by both injection and production, and pressure is maintained at 8–10 MPa with a small fluctuation amplitude.

4. Discussion

4.1 Induced Versus Triggered

The words "induce" and "trigger" are used almost in an equivalent manner in many scientific papers on earthquakes. The commonly intended meanings are as follows. An earthquake that releases an anthropogenically induced stress is defined as induced; otherwise, if an earthquake releases tectonic stress, it is considered as triggered (McGarr et al., 2002). In some papers, the term

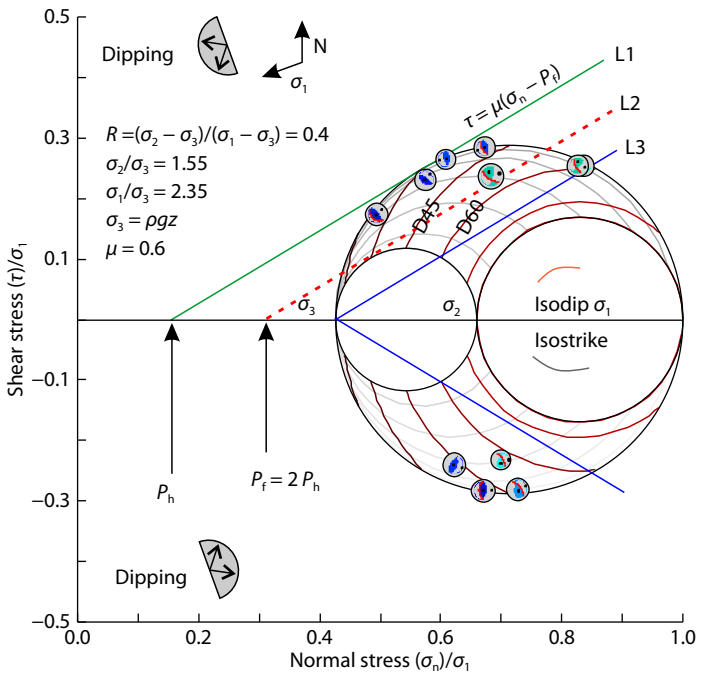

Figure 9. Focal mechanisms of $M > 4$ earthquakes are shown as a 3D Mohr diagram (normalized by the maximum principal stress, σ_1) by lower-hemisphere projection of the focal spheres. Lines L1, L2, and L3 indicate the fault strengths under hydrostatic, intermediate, and lithostatic fluid pressures, respectively.

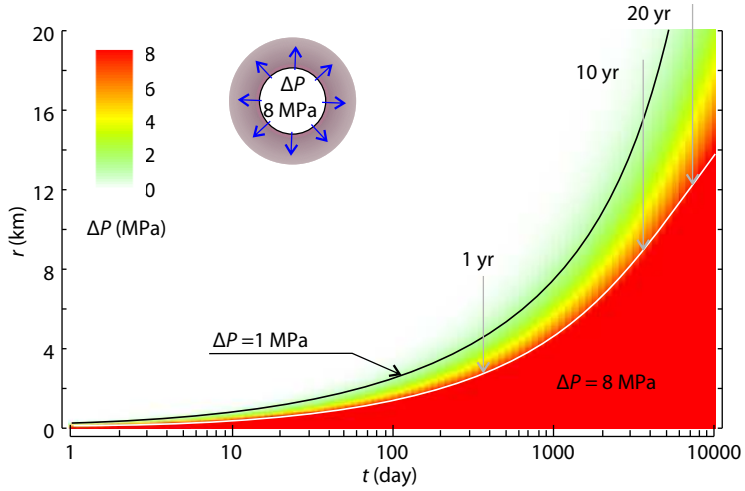

Figure 10. Pore pressure diffusion based on two-dimensional radiational flow model for a constant injection rate of 0.135 m^3/min (estimated from water loss) and constant source pressure of 8 MPa (the injection pressure was roughly kept in the range of 8–10 MPa). For maintain a constant injection rate, the source area increases over time.

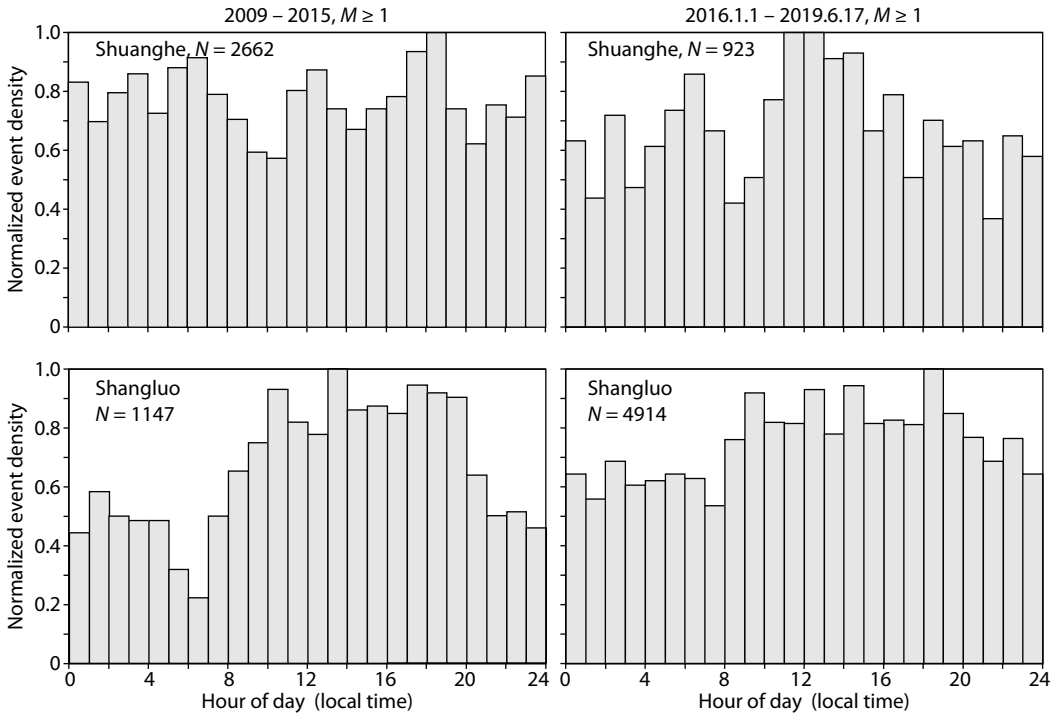

Figure 11. Stacked hourly distribution of event rate, normalized by the maximum for Shuanghe and Shangluo areas. *N* represents the total number of events.

"induced" is used to describe both sources of accumulated stress (Ellsworth, 2013). Generally, it is very difficult to give a strict definition that is acceptable to the scientific community, society, and industrial operators. For the case of seismicity due to injection, the following factors must be considered. 1) The level of stress change in the source region as compared with the stress drop of the earthquake. 2) The location of the earthquake hypocenter and dimensions of the source fault relative to the zone affected by the injection. 3) Permeable channels (fractures, faults, damaged volumes, and porous layers) between the injection zone and the earthquake source. 4) How much was the occurrence time of the specified earthquake advanced by external loading such as injection, compared with the expected time without external loading?

Based on 1), if the stress change is much smaller than the stress drop of the earthquake, the earthquake can be termed as "triggered." Remote triggering by large earthquakes or tidal modulation are typical causes of triggered earthquakes. Based on 2), seismicity within an injection-affected zone is termed as induced, and activity outside the zone is triggered. Large earthquakes initiated within the injection zone that rupture faults beyond the zone

are also defined as triggered. For example, the M_W 5.5 Pohang Korea earthquake was considered to be triggered by enhanced geothermal system stimulation (Ellsworth et al., 2019). In fact, all factors mentioned above have uncertainty for any real-world seismic events. Strict definitions are sometimes impossible and outside the scope of scientific research.

In our case, major seismicity in the Shangluo shale gas area can be termed as induced or triggered seismicity. Cases of fault activation were detected from monitoring of microseismicity. After a few stages of HF, the recognized fault reached ~1 km length within the zone, enough to produce earthquakes of a magnitude greater than 4.

For the case of the Shuanghe salt mine area, seismicity here is clearly correlated with the injection history and water loss in the salt mine. We agree with the conclusion of previous studies (Ruan X et al., 2008, Sun XL et al., 2017) that earthquakes occurring before the *M*6 sequence were induced by the long-term deep well injections.

For the *M*6 main event and aftershocks, further studies are expected because many aspects remain poorly understood. The following lines of inquiry are preliminary suggestions.

As a result of long-term high-pressure water injection, the Shuanghe rock salt cavity is becoming ever larger, increasing the possibility that the dolomite layer surrounding the salt formation will become connected to the highly pressured water through both direct exposure and permeable fault zones. Because faults in brittle rocks are highly permeable zones, the overpressurized water can flow out along pre-existing faults and play a role in weakening them. This is a reasonable interpretation of the significant water loss seen at this mine and the correlation between seismic moment and volume of water loss (Sun XL et al., 2017). Moreover, a feedback mechanism between faulting and water flow has been observed to enhance fault permeability in the laboratory (Li XY et al., 2016). As the water pressure increases and the spreading front broadens, more faults with different orientations reach a critical state, providing conditions for the occurrence of earthquake swarms, such as the Changning sequence.

By ignoring the poroelastic effect due to water injection, the estimated fluid pressure required to activate a dangerous fault in the Shangluo shale gas area can be correlated with HF activities (Lei XL et al., 2019). In contrast, the estimated overpressure in the Shuanghe area ranged from 0.1 to 67 MPa. Five of 10 events showed an overpressure of less than 10 MPa, which could be explained by the long-term deep well injection because the maximum injection pressure is ~10 MPa. For other earthquakes having a deeper focal depth or unfavorable fault orientation and dip angle, a reasonable interpretation requires other factors. Possible factors include stress inhomogeneity and overpressurized fluid in deeper reservoirs. In the Sichuan Basin, overpressurized natural gas reservoirs are not rare. For example, the 2010 *M*5.1 Suining earthquake, an isolated event, is suggested to have been triggered through fault-valve behavior by episodic gas flow from overpressurized aquifers (Lei XL et al., 2017a). In any case, many aspects are worthy of further investigation.

4.2 When an Injection-Induced Earthquake is as Large as Expected, What Can We Do?

On the whole, the maximum magnitudes observed in the study areas are as large as statistically expected from the Gutenberg–Richter relationship between frequency and magnitude, in agreement with observations at other sites (Van Der Elst et al., 2016). However, at the local level, some of the largest events are outliers of the power law of seismicity observed thus far. The mechanisms and conditions for such extreme events, most of which are destructive, are important and emerging issues for further study.

The insights in this article are preliminary, and it is difficult to reach consensus in both academic and social circles. The production of well salt in the Shuanghe area is important and has a history of nearly 2,000 years. Modern industrialized production through deep well injection has continued for more than 30 years and indeed has contributed greatly to the development of the local economy. However, salt well production is not an indispensable industry for the country or the local community. It is necessary to take some emergency measures, for example, to reduce the impact of water injection activities on surrounding faults by reducing the injection pressure. At the same time, research focusing on injection-induced earthquakes in a deep-well salt mining environment should be greatly promoted to investigate the generation, characteristics, and mechanisms of seismicity induced by deep mining from multiple aspects through different research techniques. It is an emerging scientific challenge to explore feasible solutions to establish a foundation for safe and effective deep salt mining. The Shuanghe salt mine is an ideal setting for such seismological research, and this site could be valuable as an experimental field.

As for the shale gas area, it is an imperative to develop the shale gas industry, which is one of China's strategic objectives. However, the geological conditions of the Sichuan Basin are special, the tectonic environment is variable, and the induced seismic risk assessment and countermeasures of the shale gas mining process are seriously insufficient. The increasing seismic event frequency, including destructive earthquakes, has caused significant disasters and economic losses. It is necessary to increase the investment for corresponding scientific research, to study the conditions that induce destructive earthquakes, and thus to develop effective solutions for assessment and mitigation of risks related to induced earthquakes — in summary, an emerging scientific challenge requiring close cooperation between the three parties of government, industry, and academy.

5. Conclusion

Following previous studies, this paper makes a comparative study focusing on the potential link between injection and seismicity in the Shuanghe salt mine area and the adjacent Shangluo shale gas area. The series of evidence chains evaluated here included timing of seismic activity, location of earthquakes, the mode of occurrence in the statistical model, inversion of stress field patterns, and fault reactivation analysis. These indicate that seismic activities, including a number of destructive $M \geq 5$ earthquakes, in both areas were tectonic earthquakes that occurred as a result of fault

activation induced by fluid injection for either salt or shale gas production.

At first, following systematic fracturing in horizontal wells since the end of 2014, seismicity in the Shangluo area showed a progressively increasing background with fluctuations. Earthquakes were clustered around active HF wells. Each individual cluster was initiated soon after the start of HF and decayed quickly after the end of HF operations. Between 2015 and the end of August 2019, 11 $M \geq 4.0$ events (including 3 $M \geq 5.0$) had been observed. The centroid depths of $M \geq 4.0$ earthquakes and some well-determined clusters were distributed in a depth range from ~1 to ~5 km, with a peak just below the target shale formation. We thus conclude that the observed seismicity in the Shangluo shale gas area has resulted from reactivation of pre-existing faults induced by hydraulic fracturing. The Xingwen *M*5.7 earthquake that occurred on 18 Dec. 2018 was an extreme event, with a magnitude greater than that expected from the statistical model obtained from the area's seismic history. Not surprisingly, it was initiated in the zone of treatment but ruptured (probably unidirectionally) beyond the zone along a direction of 10 deg NW. At the same time, the NW-extending structure of the Changning anticline likely played a role in arresting the rupture.

The epicenter of the *M*6 Changning earthquake was located in the salt mine well area. From the 1970s to the mid-1980s, no earthquakes of magnitude 4 or higher were observed within the Changning anticline structures. The few earthquakes might represent background seismicity, or they may have been induced by the beginning of drilling activities. Over the past 30 years, fresh water has been extensively injected through several deep wells with a depth of 2,700–3,000 m at a pressure of 8–10 MPa for salt mining. After the start of injection, especially after the start of cross-well injection and production through horizontal docking, the event rate and the maximum magnitude demonstrated an increasing tendency.

Until 2014, major seismicity was limited in the Changning anticline. Since then, until the occurrence of the *M*6 earthquake, major seismicity in the Shuanghe area followed a slightly increasing event rate until the *M*5.7 Xingwen earthquake occurred in the north part of the Shangluo shale gas area. The *M*5.7 event increased the event rate in the Shuanghe area by several times. Many more earthquakes clustered on the east side of the salt field and extended along the NNW direction, indicating activation of NNW structures; NNW is also the major direction of lineation in the shale gas area. We agree with the conclusions of previous studies (e.g., Sun et al., 2017) that the seismicity here was induced by deep well injections for salt mining.

Acknowledgments

The GIS-based data processing software package GeoTaos was used for statistical analysis, hypocenter relocation, and moment tensor inversion through embedded utilities, stress inversion, overpressure estimation, and CFS calculation. This package is available for free at https://staff.aist.go.jp/xinglin-lei/. The maps and plots were created using the free software GeoTaos_map (developed by Xinglin Lei; https://staff.aist.go.jp/xinglin-lei/) and finished with the software CorelDRAW X8 (©2016 Corel Corp.). The background topography in the maps is based on the ALOS World 3D-30m (AW3D30) digital elevation model data (https://www.eorc.jaxa.jp/ALOS/aw3d30/index_j.htm).

We thank two anonymous reviewers and an editor for their detailed and timely review comments. Wang acknowledges support from the State Scholarship Fund of China (No. 201804190004).

References

Atkinson, G. M., Eaton, D. W., Ghofrani, H., Walker, D., Cheadle, B., Schultz, R., Shcherbakov, R., Tiampo, K., Gu, J., … Kao, K. (2016). Hydraulic fracturing and seismicity in the western Canada Sedimentary Basin. *Seismol. Res. Lett.*, *87*(3), 631–647. https://doi.org/10.1785/0220150263

Barker, J. A. (1988). A generalized radial flow model for hydraulic tests in fractured rock. *Water Resour. Res.*, *24*(10), 1796–1804. https://doi.org/10.1029/WR024i010p01796

Båth, M. (1965). Lateral inhomogeneities of the upper mantle. *Tectonophysics*, *2*(6), 483–514. https://doi.org/10.1016/0040-1951(65)90003-X

CENC (2018). Figure collection of 16 December 2018 Xingwen *M*5.7 earthquake (in Chinese). https://mp.weixin.qq.com/s/4kff7rNwcl-XnjyYN2h4lQ (last accessed Jan. 2019).

Ellsworth, W. L. (2013). Injection-induced earthquakes. *Science*, *341*(6142), 1225942. https://doi.org/10.1126/science.1225942

Ellsworth, W. L., Giardini, D., Townend, J., Ge, S. M., and Shimamoto, T. (2019). Triggering of the Pohang, Korea, Earthquake (M_w 5.5) by Enhanced Geothermal System Stimulation. *Seismol. Res. Lett.*, *90*(5), 1844–1858. https://doi.org/10.1785/0220190102

Gephart, J. W., and Forsyth, D. W. (1984). An improved method for determining the regional stress tensor using earthquake focal mechanism data: application to the San Fernando earthquake sequence. *J. Geophys. Res.*: *Solid Earth*, *89*(B11), 9305–9320. https://doi.org/10.1029/JB089iB11p09305

Hardebeck, J. L., and Michael, A. J. (2006). Damped regional-scale stress inversions: methodology and examples for southern California and the Coalinga aftershock sequence. *J. Geophys. Res.*: *Solid Earth*, *111*(B11), B11310. https://doi.org/10.1029/2005JB004144

Lei, X. L., Yu, G. Z., Ma, S. L., Wen, X. Z., and Wang, Q. (2008). Earthquakes induced by water injection at ~3 km depth within the Rongchang gas field, Chongqing, China. *J. Geophys. Res.*: *Solid Earth*, *113*(B10), B10310. https://doi.org/10.1029/2008jb005604

Lei, X. L., Ma, S. L., Chen, W. K., Pang, C. M., Zeng, J., and Jiang, B. (2013). A detailed view of the injection-induced seismicity in a natural gas reservoir in Zigong, southwestern Sichuan Basin, China. *J. Geophys. Res.*: *Solid Earth*, *118*(8), 4296–4311. https://doi.org/10.1002/jgrb.50310

Lei, X. L., Li, X. Y., Li, Q., Ma, S. L., Fu, B. H., and Cui, Y. X. (2014). Role of immature faults in injection-induced seismicity in oil/gas reservoirs—A case study of the Sichuan Basin, China. *Seismol. Geol.* (*in Chinese*), *36*(3), 625–643. https://doi.org/10.3969/j.issn.0253-4967.2014.03.007

Lei, X. L., Ma, S. L., Wang, X. L., and Su, J. R. (2017a). Fault-valve behaviour and episodic gas flow in overpressured aquifers – evidence from the 2010 Ms5.1 isolated shallow earthquake in Sichuan Basin, China. *Prog. Comput. Fluid Dyn.*, *17*(1), 2–12. https://doi.org/10.1504/PCFD.2017.081714

Lei, X. L., Huang, D. J., Su, J. R., Jiang, G. M., Wang, X. L., Wang, H., Guo, X., and Fu, H. (2017bb). Fault reactivation and earthquakes with magnitudes of up to Mw.7 induced by shale-gas hydraulic fracturing in Sichuan Basin. *China. Sci. Rep.*, *7*(1), 7971. https://doi.org/10.1038/s41598-017-08557-y

Lei, X. L., Wang, Z. W., and Su, J. R. (2019). The December 2018 M_L 5.7 and January 2019 M_L 5.3 earthquakes in South Sichuan Basin induced by shale gas hydraulic fracturing. *Seismol. Res. Lett.*, *90*(3), 1099–1110. https://doi.org/10.1785/0220190029

Leonard, M. (2010). Earthquake fault scaling: self-consistent relating of rupture length, width, average displacement, and moment release. *Bull. Seismol. Soc. Am.*, *100*(5A), 1971–1988. https://doi.org/10.1785/0120090189

Li, X. Y., Lei, X. L., and Li, Q. (2016). Injection-induced fracturing process in a

tight sandstone under different saturation conditions. *Environ. Earth Sci.*, *75*(23), 1466. https://doi.org/10.1007/s12665-016-6265-2

McGarr, A., Simpson, D., and Seeber, L. (2002). Case histories of induced and triggered seismicity. *Int. Geophys.*, *81*, 647–661. https://doi.org/10.1016/S0074-6142(02)80243-1

McGarr, A. (2014). Maximum magnitude earthquakes induced by fluid injection. *J. Geophys. Res.*: *Solid Earth*, *119*(2), 1008–1019. https://doi.org/10.1002/2013JB010597

Meng, L. Y., McGarr, A., Zhou, L. Q., and Zang, Y. (2019). An investigation of seismicity induced by hydraulic fracturing in the Sichuan Basin of China based on data from a temporary seismic network. *Bull. Seismol. Soc. Am.*, *109*(1), 348–357. https://doi.org/10.1785/0120180310

Michael, A. J. (1987). Use of focal mechanisms to determine stress: a control study. *J. Geophys. Res.*: *Solid Earth*, *92*(B1), 357–368. https://doi.org/10.1029/JB092iB01p00357

Okada, Y. (1992). Internal deformation due to shear and tensile faults in a half-space. *Bull. Seismol. Soc. Am.*, *82*(2), 1018–1040.

Ren, R., Qian, B., Zhang, J., Zhuo, Z. C., and Qiao, L. (2015). Practice and understanding of industrial fracturing for shale gas of Longmaxi Formation in Changning region. *Oil Drill. Prod. Technol.* (*in Chinese*), *37*(4), 96–99. https://doi.org/10.13639/j.odpt.2015.04.025

Ruan, X., Cheng, W. Z., Zhang, Y. J., Li, J., and Chen, Y. (2008). Research of the earthquakes induced by water injections in salt mines in Changning, Sichuan. *Earthq. Res. China* (*in Chinese*), *24*(3), 226–234. https://doi.org/10.3969/j.issn.1001-4683.2008.03.004

Sun, X. L., Yang, P. T., and Zhang, Z. W. (2017). A study of earthquakes induced by water injection in the Changning salt mine area, SW China. *J. Asian Earth Sci.*, *136*, 102–109. https://doi.org/10.1016/j.jseaes.2017.01.030

Terakawa, T., Miller, S. A., and Deichmann, N. (2012). High fluid pressure and triggered earthquakes in the enhanced geothermal system in Basel, Switzerland. *J. Geophys. Res.*: *Solid Earth*, *117*(B17), B07305. https://doi.org/10.1029/2011jb008980

Utsu, T. (1961). A statistical study on the occurrence of aftershocks. *Geophys. Mag.*, *30*, 521–605.

Van Der Elst, N. J., Page, M. T., Weiser, D. A., Goebel, T. H. W., and Hosseini, S. M. (2016). Induced earthquake magnitudes are as large as (statistically) expected. *J. Geophys. Res.*: *Solid Earth*, *121*(6), 4575–4590. https://doi.org/10.1002/2016JB012818

Waldhauser, F., and Ellsworth, W. L. (2000). A double-difference earthquake location algorithm: method and application to the northern Hayward fault, California. *Bull. Seismol. Soc. Am.*, *90*(6), 1353–1368. https://doi.org/10.1785/0120000006

Yi, G. X., Long, F., Liang, M. J., Zhao, M., Wang, S. W., Guan, Y., Qiao, H., and Su, J. (2019). Focal mechanism solutions and seismogenic structure of the 17 June 2019 M_S6.0 Sichuan Changning earthquake sequence. *Chin. J. Geophys.* (*in Chinese*), *62*(9), 3432–3447. https://doi.org/10.6038/cjg2019N0297

Zhang, Z. W., Cheng, W. Z., Liang, M. J., Wang, X. S., Long, F., Xu, Y., Chen, W. K., and Wang, S. Y. (2012). Study on earthquakes induced by water injection in Zigong-Longchang area, Sichuan. *Chin. J. Geophys.* (*in Chinese*), *55*(5), 1635–1645. https://doi.org/10.6038/j.issn.0001-5733.2012.05.021

Zheng, X. F., Yao, Z. X., Liang, J. H., and Zheng, J. (2010). The role played and opportunities provided by IGP DMC of China National Seismic Network in Wenchuan earthquake disaster relief and researches. *Bull. Seismol. Soc. Am.*, *100*(5B), 2866–2872. https://doi.org/10.1785/0120090257

Zhu, L. P., and Ben-Zion, Y. (2013). Parametrization of general seismic potency and moment tensors for source inversion of seismic waveform data. *Geophys. J. Int.*, *194*(2), 839–843. https://doi.org/10.1093/gji/ggt137

Zou, C. N., Dong D. H., Wang, Y. M., Li X. J., Huang, J. L., Wang, S. F., Guan, Q. Z., Zhang, C. C., Wang, H. Y., ... Qiu, Z. (2015). Shale gas in China: Characteristics, challenges and prospects (I). *Petroleum Exploration and Development*, *42*(6), 753–767. https://doi.org/10.1016/S1876-3804(15)30072-0